Journal of Physiology (1990), **426**, *pp.* 145–176
With 12 figures
Printed in Great Britain

VOLTAGE DEPENDENCE AND STABILITY OF THE GATING KINETICS OF THE FAST CHLORIDE CHANNEL FROM RAT SKELETAL MUSCLE

BY D. S. WEISS AND K. L. MAGLEBY

From the Department of Physiology and Biophysics, University of Miami School of Medicine, PO Box 016430, Miami, FL 33101, USA

(*Received 4 September 1989*)

SUMMARY

1. The voltage dependence and stability of the gating kinetics of the fast Cl^- channel in excised patches of membrane from cultured rat skeletal muscle were studied with the patch clamp technique. Up to 10^6 open and shut intervals were analysed from each of five different patches containing a single fast Cl^- channel.

2. To test for kinetic stability, plots of the mean durations of consecutive groups of 5–500 open and shut intervals were examined at each voltage. After excluding infrequent entries into both an apparent subconductance state and a long-lived (inactive) shut state, there were no abrupt and sustained changes in the moving means, indicating the absence of obvious shifts to other kinetic modes. The moving means did, however, fluctuate about the overall mean.

3. A comparison of experimental and simulated data indicated that most, but not all, of the fluctuation in the moving means was due to the stochastic variation inherent in the gating process. The fluctuation not accounted for by stochastic variation was mainly expressed as a slow, low-amplitude, component of drift about the mean. This slow component was unlikely to have arisen from measurement errors.

4. To examine whether the slow drift reflected detectable changes in kinetic modes, the data were divided into consecutive groups of 50000 intervals. The exponential components describing the distributions were remarkably similar among the different groups, with stochastic variation accounting for most of the observed differences. This finding implies a single kinetic mode throughout the experiment. Thus, any changes in channel activity associated with the slow drift would have little effect on the analysis of gating kinetics presented here.

5. Depolarization increased channel open probability, P_{open}, for all five channels. This increase had a voltage sensitivity of 17 ± 4 mV per e-fold change (effective gating charge of $1{\cdot}6 \pm 0{\cdot}32$ electronic charges at 23 °C). P_{open} was 0·5 at -31 ± 4 mV.

6. The depolarization-induced increase in P_{open} typically arose from a decrease in the mean shut time (19 ± 4 mV per e-fold change; effective gating charge of $1{\cdot}3 \pm 0{\cdot}3$ at 23 °C) and an increase in the mean open time (109 ± 61 mV per e-fold change; effective gating charge of $-0{\cdot}24 \pm 0{\cdot}13$).

7. Neither plots of P_{open} *versus* voltage nor plots of the mean open and mean shut time *versus* voltage were completely described by a single Boltzmann distribution, suggesting multiple voltage-sensitive steps in channel gating.

8. The number of exponential components in the open and shut dwell-time distributions (typically two open and six shut) were independent of membrane potential (examined range: −30 to −100 mV), suggesting that the voltage dependence of P_{open} does not result from a voltage-dependent change in the effective number of kinetic states.

9. The typical effect of depolarization on the open dwell-time distribution was to increase the time constants of both exponential components and shift area from the fast to the slow component.

10. The typical effect of depolarization on the shut dwell-time distribution was to decrease the time constants of all six components and shift net area from the four slower to the fastest component.

11. For one of the five channels the observed mean open time decreased, rather than increased, with depolarization. This reversed voltage sensitivity of the observed mean open time may actually reflect a reversed voltage sensitivity of a rate away from a shut state. In addition, there were some differences in some of the other kinetic parameters among the channels. These differences suggest some kinetic heterogeneity, but the heterogeneity was small relative to the overall similarity in gating kinetics of the five channels.

12. The typical results suggest a kinetic scheme for the normal activity of the fast Cl^- channel with two open and six shut states. All kinetic states are entered at all the examined voltages, with the frequency of entry and the lifetimes of the various states shifting progressively with depolarization to generate longer mean open intervals and briefer mean shut intervals.

INTRODUCTION

Voltage-dependent ion channels initiate and modulate a variety of cellular functions (Hille, 1984). The Na^+ and K^+ channels underlying the action potential are examples from a class of channels which activate and then inactivate upon depolarization; the Na^+ channel inactivates rapidly and the K^+ channel much more slowly (Hodgkin & Huxley, 1952; Armstrong & Bezanilla, 1977; Aldrich, Corey & Stevens, 1983; Hille, 1984; Horn & Vandenberg, 1984). A second class of voltage-dependent channels includes those activated by agonists and modulated by membrane potential, such as the acetylcholine receptor channel (Magleby & Stevens, 1972; Neher & Sakmann, 1975) and the γ-aminobutyric acid gated channel (Weiss, 1988). The fast Cl^- channel from cultured skeletal muscle (Blatz & Magleby, 1985) is an example from a third class of voltage-dependent channels which differs from the preceding two classes in that it neither requires agonist for activation nor does it inactivate with depolarization. Instead, the fast Cl^- channel can be continuously active (at least in excised patches of membrane), with its open probability (P_{open}) increasing with depolarization. Little is known about the mechanism by which voltage modulates activity in this third class of channels. The purpose of this paper is to use the single-channel recording technique (Hamill, Marty, Neher, Sakmann & Sigworth, 1981) to investigate the voltage-dependent gating kinetics of the fast Cl^- channel.

In approaching this study it soon became apparent that the collection of hundreds

of thousands of open and shut intervals would be necessary to adequately define the single-channel kinetics as a function of voltage. Such large sample sizes are necessary since the gating kinetics of the fast Cl^- channel are complex, with a minimum of two open and five shut states during normal activity (Blatz & Magleby, 1986*a*, 1989). Collecting such large amounts of data from the fast Cl^- channel is possible since the channel does not inactivate with depolarization. There is no assurance, however, that the data will be sufficiently stable for analysis, as channels often change their kinetic properties with time (Patlak, Gration & Usherwood, 1979; Moczydlowski & Latorre, 1983; Hess, Lansman & Tsien, 1984; Blatz & Magleby, 1986*a*; Patlak & Ortiz, 1986; Patlak, Ortiz & Horn, 1986; McManus & Magleby, 1988; Nilius, 1988; cf. Lacerda & Brown, 1989). Thus, the first part of this study investigates the long-term kinetic stability of single fast Cl^- channels.

We find that the gating kinetics of the fast Cl^- channel can remain sufficiently stable over time to allow a detailed analysis of voltage-dependent gating. Consequently, stable data from five single fast Cl^- channels have been analysed. Although there are some kinetic heterogeneities among channels, the data are sufficiently similar to propose a general working hypothesis for the voltage-dependent modulation of the fast Cl^- channel. An abstract of some of these observations has appeared (Weiss & Magleby, 1988).

METHODS

Preparation, recording and solutions

Currents flowing through single fast Cl^- channels (Blatz & Magleby, 1985, 1986*a*) were obtained with the patch clamp technique (Hamill *et al.* 1981) from inside-out patches of surface membrane excised from primary cultures of rat skeletal muscle (myotubes). A single-channel patch was identified by current steps to a single consistent level throughout the experiment, including extended observations at high levels of activity.

Pregnant rats were killed with an overdose of ether anaesthesia. The fetuses were then removed and skeletal muscle was obtained from their limbs and cultured as described in Barrett, Barrett & Dribin (1981). Myotubes were first transferred to the main recording chamber and immersed in a bathing solution containing (in mM): NaCl, 150; KCl, 4; $MgCl_2$, 1; $CaCl_2$, 2; TES buffer (*N*-tris-hydroxymethyl-2-aminoethane sulphonic acid), 5; pH = 7·2. After excising a patch of membrane, the recording pipette with attached patch was manoeuvred into a microchamber submerged in the main chamber (Barrett, Magleby & Pallotta, 1982). The fluid level in the main chamber was then dropped below the level of the fluid in the microchamber.

The flowing solution in the microchamber, which bathed the normal intracellular surface of the membrane patch, contained (in mM): KCl, 1000; TES, 2; EGTA (ethyleneglycol-bis-(β-aminoethylether)*N*,*N*′-tetraacetic acid), 1; pH = 7·2. The solution in the patch pipette, which bathed the normal extracellular surface of the membrane, contained (in mM): KCl, 140; TES, 5; EGTA, 0·5; pH = 7·2. The free Ca^{2+} in the solutions was $< 10^{-8}$ M. Low Ca^{2+} at the inner membrane surface prevented the Ca^{2+}-activated K^+ channels from becoming active (Blatz & Magleby, 1987). The high concentration of intracellular Cl^- increased the single-channel current amplitude, which greatly increased the signal-to-noise ratio (Blatz & Magleby, 1986*a*). Experiments were performed at either 23 or 18 °C, as indicated.

Membrane potential for excised patches is defined in the standard manner for intact cells, as the potential at the normal intracellular surface minus the potential at the normal extracellular surface. Single-channel currents were collected at three to eight different membrane potentials for each of the five studied channels. To assess the stability of the experiments, data were also collected at a control membrane potential (usually −40 mV) between each of the examined potentials. Since longer periods of time were required to collect sufficient data at hyperpolarized potentials where the activity of the channel was low, data collection at the hyperpolarized potentials was

occasionally interrupted to obtain control data. Currents were recorded on a Racal 4DS tape-recorder (Racal Recorders, Vienna, VA, USA) with a bandwidth of DC to 20 or 40 kHz.

Setting the level of filtering for initial analysis

Data on tape were filtered prior to interval detection to eliminate the possibility that noise would be falsely detected as channel events. Since single-channel current amplitude varies with membrane potential, the optimal level of filtering would be different for data collected at different membrane potentials. The level of filtering for each membrane potential was determined by setting the 50% amplitude threshold for event detection (see below) on the side of the baseline opposite channel opening, and decreasing the cut-off frequency of the filter until no false events (threshold crossings by noise) were detected. Assuming symmetrical noise, then no false events should be detected when the threshold was set the same absolute distance from the baseline on the side of channel opening (McManus, Blatz & Magleby, 1987).

The level of filtering is expressed in terms of the dead time, measured as the duration of the briefest interval that would be detectable with 50% amplitude threshold detection (Colquhoun & Sigworth, 1983). Dead times ranged from 58–19 μs (effective cut-off frequencies of 3·1–9·5 kHz). The dead times for Figs 1*B* and 2–5 were: 45·2, 36·3, 27·2 and 23·2 μs for potentials of −20, −40, −60 and −80 mV, respectively. When data at different membrane potentials were to be compared, they were numerically refiltered to the same level (details below).

Measuring open and shut interval durations

The durations of open and shut intervals were measured by computer with 50% amplitude threshold detection (Colquhoun & Sigworth, 1983). For this procedure, the tape-recorder was slowed to 1/8–1/32 of the original recording speed in order to give the DEC 11/73 computer (Digital Equipment Corp., Marlboro, MA, USA) sufficient time to sample, detect and store the interval durations. While playing the data into the computer, the single-channel currents were simultaneously inspected on an oscilloscope to check for baseline drift and noise artifacts. The effective sampling interval used for computer analysis ranged from 2–8 μs. The output of the 50% threshold detection was a sequential file of open and shut interval durations. The precautions used to prevent errors which can arise from threshold analysis (Colquhoun, 1988) are detailed elsewhere (McManus & Magleby, 1988, 1989).

Assessing experimental stability and calculation of P_{open}

Steps were taken to insure that the data analysed were stable and represented activity in the normal gating mode (Blatz & Magleby, 1986*a*). First, stability plots of the running means of consecutive open and shut interval durations were constructed at several different levels of resolution for each membrane potential. The resolution was determined by the number of intervals averaged. For a stability plot of open intervals the durations of the first 5–500 sequential open intervals, depending on the desired resolution, were averaged, then the next 5–500 open intervals were averaged, and the process repeated until the end of the file was reached. The averages were then plotted against the open interval number. Similar averaging of sequential shut interval durations gave stability plots of shut intervals.

Sojourns to kinetic modes other than normal were identified from changes in the means in the stability plots (Blatz & Magleby, 1986*a*; McManus & Magleby, 1988) and removed from the files. Also, infrequent excursions to an apparent subconductance state, with amplitude about one-half of the main conductance state, were identified as a simultaneous decrease in the mean open and shut interval durations in high-resolution stability plots (averages of 5–50 intervals). This decrease comes about because the current during the subconductance state straddles, and therefore repeatedly traverses, the 50% threshold for event detection, causing a series of false open and shut intervals of brief duration (Colquhoun, 1988). False events arising from the apparent subconductance state were removed from the files and excluded from further analysis.

The open probability P_{open} (fraction of time a channel spends open) was determined from the files containing the measured durations of open and shut intervals by dividing the sum of the durations of the open intervals by the sum of the durations of the open plus shut intervals.

Numerical refiltering of the open and shut interval durations

In order to distinguish the effects of voltage on channel kinetics from the effects of filtering, it is necessary to examine all the data at a similar level of filtering. We have employed a numerical

method of refiltering the measured intervals to allow analysis of the same data at different levels of filtering, without the very time-intensive process of reanalysing the original current records.

The files of interval durations obtained at the different voltages were numerically refiltered to give the same dead time for all voltages, with the dead time equivalent to or slightly greater than the dead time of the most heavily filtered current record in the experiment. The numerical refiltering was performed by scanning the sequential arrays of open and shut intervals and combining each interval less than the selected dead time with the durations of the immediately preceding and following (adjacent) intervals. For instance, if the selected dead time was 0·05 ms, a sequence of open, shut, open,... interval durations before numerical refiltering, such as 1·5, 3·2, 0·04, 1·0, 2·1 would become: 1·5, 4·24, 2·1 after numerical refiltering.

Numerical refiltering of this type would not be expected to give the same result as standard filtering of all the original current records at the same level, because of the infinite roll-off frequency of the numerical filter, and because with normal active filtering currents from intervals with durations less than the dead time can sum and be detected. The errors associated with numerical refiltering were examined by analysing the same current record with two different levels of active filtering to yield two different dead times. The sequential files of measured open and shut interval durations were then numerically refiltered to the same dead time. Dwell-time distributions of open and shut intervals were constructed from the numerically refiltered files, and the distributions fitted with sums of exponentials.

The number of detected exponential components was not altered by numerical refiltering, and estimates of the areas and time constants of the exponential components were typically within 6% for the two files numerically refiltered to the same level. In some tests, however, differences for the fastest shut component could be as great as 10–25% for data at hyperpolarized membrane potentials where the area of the fastest shut component was small. Thus, numerical refiltering is not without error, but in most cases the anticipated errors from numerical refiltering were less than those expected from stochastic variation, and thus would have little effect on the results of this study. The dead times used in the numerical refiltering for Figs 6, 7 and 9–12 were: 0·0363 μs for channels 1–3, 0·0463 μs for channel 4, and 0·0581 μs for channel 5. Data for channel 4 were also numerically refiltered at 0·0581 μs, and similar conclusions were obtained.

Binning, fitting and plotting dwell-time distributions

The methods used to bin, fit and plot the dwell-time distributions have been described in detail previously (Blatz & Magleby, 1986*a*, *b*; McManus *et al.* 1987). Briefly, the open and shut interval durations were binned as the logarithm of their duration with a resolution of fifty bins per log unit. It was these high resolution distributions which were fitted. When plotting the dwell-time distributions some of the bins were combined so that adjacent points would not overlap, and for Fig. 4 the data were rebinned at a resolution of 10 bins per log unit for plotting.

The distributions of open and shut interval durations were fitted with sums of exponentials using maximum-likelihood fitting techniques (Colquhoun & Sigworth, 1983; McManus *et al.* 1987). The calculated distributions were described by

$$f(t) = \sum_{j=1}^{k} a_j \tau_j^{-1} \exp(-t/\tau_j), \quad (1)$$

where $f(t)$ is the probability density function, k is the number of exponential components, and τ_j and a_j are the time constant and area, respectively, of component j. The fits were started at twice the dead time to prevent the introduction of phantom components (Roux & Sauve, 1985; Blatz & Magleby, 1986*b*). The likelihood ratio test (Rao, 1973; Horn & Lange, 1983; McManus & Magleby, 1988) was then used to determine the number of exponential components describing each distribution, with the stringent criterion of $P < 0{\cdot}01$ for an addition component to be significant.

Using simulation to estimate stochastic variation

Simulated data were used to estimate the variability contributed to the experimental data by stochastic variation. The most likely rate constants for scheme I (with state C_8 deleted) were first obtained from the experimental distributions of open and shut times as detailed in Blatz & Magleby (1986*a*). These rate constants were then used to generate files of simulated open and shut interval durations with filtering the same as that for the experimental data (details in Blatz & Magleby, 1986*b*). The files of simulated intervals were then analysed in the same manner as used

to analyse the experimental data. The variability in the simulated data should then give an estimate of the variability expected in the experimental data due solely to stochastic variation for Fig. 2*C* and *D* and due to both stochastic variation and fitting errors for Fig. 5.

Using resampling to estimate errors in fitting

Resampling methods (Efron, 1982; Horn, 1987) were used to obtain estimates of fitting errors associated with determining the time constants and areas of the exponential components and the voltage sensitivities of these parameters. Such fitting errors mainly reflect the uncertainty in the estimates arising from limited sample sizes and the fact that some of the parameters may not be well defined. To estimate these fitting errors the experimental open and shut dwell-time distributions at each voltage were resampled to obtain artificial distributions for each channel. Each artificial distribution was generated by randomly drawing (with replacement) individual intervals from an original distribution. Thus, for each artificial distribution, some of the original intervals may appear more than once and some may not appear at all. This procedure was repeated to obtain five complete artificial data sets for each channel. Each of the artificial data sets was then analysed in the exact same manner as used for the original data sets, including the fitting with eqns 5 and 7. The standard deviations obtained from analysis of the five artificial data sets are the error bars plotted in Figs 7, 10 and 12, and include fitting errors associated with estimation of the parameters.

To examine if observed differences in parameters among the different channels were greater than the errors in the estimates of the parameters, Gaussian distributions were generated based on the means and standard deviations determined by resampling. If the overlap in area of the Gaussian distributions for two compared parameters was less than 1%, then the observed difference in the parameters was assumed not to arise from the limited number of analysed intervals and fitting errors.

Such an application of resampling can designate a difference as significant when it is not. The reason for this is that resampling, as applied above, mainly estimates fitting errors associated with determining the parameters from the given data sets, and does not necessarily take into account other sources of variability, such as stochastic variation, which is contributed to the data sets before they are resampled.

RESULTS

Single-channel currents at different membrane potentials

Figure 1 shows currents through a single fast Cl^- channel for membrane potentials ranging from -20 to -80 mV. Currents are presented on slow (*A*) and fast (*B*) time bases for each voltage, with downward current steps indicating channel opening. The voltage dependence of the gating kinetics is readily apparent; channel open probability, P_{open}, increases with depolarization. In order to investigate the mechanism of this voltage dependence, large numbers of open and shut intervals were collected to define the kinetics at the different voltages. Data from five single-channel patches were analysed separately so that possible kinetic heterogeneity among the channels could be examined. The number of events analysed for channels 1–5 in this paper were 1040270, 297750, 567010, 148070 and 311700, respectively.

The meaningful analysis of such large numbers of events requires that channel kinetics remain stable during the extended periods of time required to collect the data, and that the applied voltages do not have long-lasting kinetic effects beyond their durations.

Stability plots of mean open and shut interval durations

The long-term stability of channel gating was initially assessed by collecting single-channel currents at a control voltage (typically -40 mV) between each of

the various test voltages. An observation of unstable open or shut mean interval durations would then suggest unstable gating.

The records in Fig. 1 are from channel 1 in which more than 10^6 intervals were collected over a 25 min period. Of the total, 585000 were obtained during the periodic steps to the control voltage of −40 mV. Figure 2 presents stability plots for

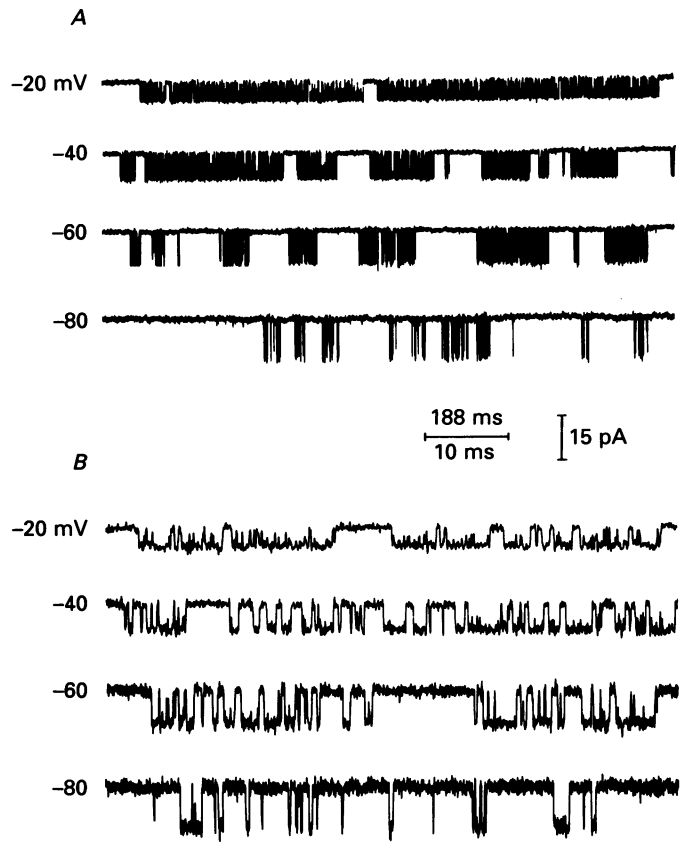

Fig. 1. Currents through a single fast Cl^- channel in an excised membrane patch from cultured rat skeletal muscle. Data are presented for four different membrane potentials on slow (*A*) and fast (*B*) time bases. Inward (downward) current steps indicate channel opening. The effective filtering in *A* was 2·4 kHz for all voltages. Filtering for *B* in Methods. The data in this and the remaining figures are from channel 1 unless otherwise indicated.

this control data. In *A* the mean open interval duration is plotted against the sequential open interval number. *B* presents a similar plot for the shut intervals. The moving means are for sequential blocks of 500 intervals, and the grand mean of the 292500 intervals in each plot is indicated by a dotted line and arrow.

Figure 2*A* shows that the mean open interval duration at −40 mV for data collected periodically throughout the entire experiment remains relatively stable, but that there is an apparent slow drift of small magnitude about the grand mean. The plot of the mean shut interval duration in *B* also shows a slow drift, but this drift

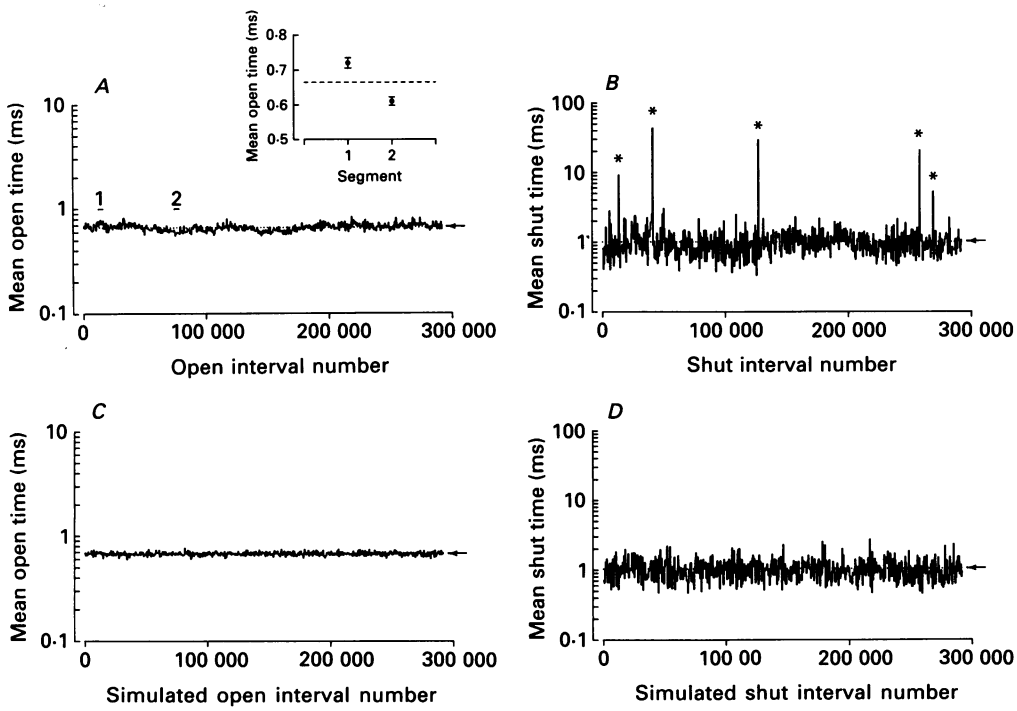

Fig. 2. Stability plots of the moving mean durations of open and shut times. *A* and *B*, experimental data. Single-channel currents were collected at membrane potentials ranging from −30 to −90 mV. To test for stability the potential was periodically stepped to a control potential of −40 mV. Of the 1040270 intervals collected in this experiment, 585000 were obtained at −40 mV. Successive open and shut intervals for data collected at −40 mV were averaged separately, 500 at a time, and the open means plotted against successive open interval number in *A* and the shut means plotted against successive shut interval number in *B*. The dashed lines and arrows indicate the grand means of the 292500 open intervals in *A* and the 292500 shut intervals in *B*. The insert in *A* shows the means and standard deviations of seven separate reanalyses of the original current record for data segments marked by the bars labelled 1 and 2. The asterisks in *B* mark shut means in which one of the 500 averaged shut intervals was exceedingly long, presumably due to entry into an inactive shut state. The durations of the single long shut intervals were (from left to right): 4·11, 21·4, 13·7, 9·81 and 2·15 s. *C* and *D*, predicted stability plots for scheme I (in the Discussion, with state C_8 deleted) with the following rate constants (s^{-1}): 1−3, 2512; 2−4, 3419; 3−1, 19849; 3−4, 14602; 4−2, 331·6; 4−5, 740·2; 5−4, 1870; 5−6, 259·5; 6−5, 570·4; 6−7, 277·2; 7−6, 25·12.

is partially masked by the fluctuation between the successive means. The greater fluctuation is expected because the shut dwell times span several orders of magnitude greater range of durations than the open dwell times (see below). The shut interval stability plot also suggests a slow drift about the overall mean. Excluded from the stability plots in Fig. 2 are the data obtained during steps to voltages other than −40 mV. The slow drift appeared independent of the voltage steps, since the moving means for data collected just before and after the voltage steps were not discontinuous.

The asterisks in the shut interval stability plot (Fig. 2*B*) indicate five means of 500

shut intervals which are markedly greater than the others. In each case the mean was elevated because one of the averaged shut intervals was excessively long (2–21 s, values in figure legend). These long shut intervals reflect entry into an inactive shut state and contribute less than 0·0001–0·00001 to the total area of the shut distribution (Blatz & Magleby, 1986*a*). The frequency of occurrence of these inactive shut intervals remained low at all the examined voltages. Because the inactive shut intervals occurred too infrequently for detailed study, they were excluded from further analysis.

Two types of variability in the stability plots

The variability in the stability plots in Fig. 2*A* and *B* appears to be of two types: a stepwise change between the means of each 500 successive intervals and, as mentioned earlier, a slow drift about the grand mean. Simulation was used to investigate to what extent these two types of observed variability might arise from the stochastic variation inherent in channel gating. Figure 2*C* and *D* presents stability plots of simulated data generated by a kinetic scheme with two open and five shut states. The kinetic scheme, which had no inactive shut state, is defined by scheme I (as given in Discussion, but with state C_8 deleted). Such a scheme has previously been shown to describe the gating of the fast Cl^- channel at a single voltage (Blatz & Magleby, 1986*a*, 1989). The simulated stability plots in *C* and *D* then indicate the expected stochastic variation for a stable (time homogeneous) gating mechanism.

Visual comparison of the experimental and simulated stability plots (Fig. 2) shows that much of the observed variability in the experimental data is consistent with stochastic variation. Nevertheless, the experimental open interval stability plot in *A* appears to have more stepwise variability than the simulated stability plot in *C*. The experimental open interval stability plot also has a slow drift not present in the simulated stability plot. The experimental shut interval stability plot in *B* appears to display similar stepwise variability as the simulated stability plot in *D*, if the five long means reflecting entry into the inactive shut state are excluded. The experimental shut interval stability plot also appears to display somewhat more slow drift. To quantify these apparent differences between the experimental and simulated stability plots, two methods were employed. In the first, the average absolute stepwise variability between the consecutive means of each 500 intervals was calculated from

$$\text{stepwise variability} = \sum_{i=1}^{N-1} |u_i - u_{i+1}|/(N-1), \tag{2}$$

where u_i represents the mean of the ith set of 500 consecutive interval durations, and N is the total number of sets of 500 consecutive interval durations. The stepwise variability calculated in this manner would be relatively insensitive to slow drift.

In the second method, the overall variability was calculated from the average absolute distance between each mean of 500 intervals and the grand mean with

$$\text{overall variability} = \sum_{i=1}^{N} |u_g - u_i|/N, \tag{3}$$

where u_g represents the grand mean of all 292 500 open or shut intervals. This second method measures the deviation of the individual means of 500 intervals from the grand mean, and hence detects both step changes and slow drift.

The results of applying eqns (2) and (3) to compare the simulated and experimental stability plots in Fig. 2 are given in Table 1. Almost all of the variability in the shut interval stability plot during normal activity (inactive shut intervals excluded) can be accounted for by stochastic variation. The simulated variability accounted for 96 and 94 % of the experimental stepwise and overall shut variability, respectively. The stepwise shut variability, however, may be sufficiently large to mask the apparent slow drift. Table 1 also shows that stochastic variation accounts for most (80 %) of the experimentally observed stepwise variability in the open interval stability plot. However, as was apparent from visual observation, the slow drift in the open interval stability plot was greater than expected from stochastic variation alone; the simulated overall open variability only accounted for 55 % of the experimental overall open variability.

TABLE 1. Variability of experimental and simulated stability plots

	Stepwise variability (ms)			Overall variability (ms)		
	Experimental	Simulated	Simulated/ Experimental	Experimental	Simulated	Simulated/ Experimental
Open	0·041	0·033	0·80	0·040	0·022	0·55
Shut	0·413	0·395	0·96	0·298	0·281	0·94

The stepwise and overall variability were calculated from the data in Fig. 2 with eqns (2) and (3), respectively. The five shut means indicated by the asterisks in Fig. 2*B* were excluded.

Slow drift in the open stability plot is not due to measurement error

To determine whether the slow drift in the open stability plot might have arisen from incorrect threshold settings or baseline drift, both of which could change the numbers of detected events, and hence the mean interval duration, the two segments of data under the bars labelled 1 and 2 in Fig. 2*A* (8000 total events) were reanalysed from the original current records independently by both investigators. The mean open interval durations and standard deviations for seven separate complete reanalyses are shown in the inset in Fig. 2*A* on a greatly expanded ordinate. The dashed line indicates the grand mean of all open intervals from Fig. 2*A*. The means of segments 1 and 2 were significantly different from each other ($P \ll 0{\cdot}001$). These results indicate that the observed drift in the open stability plot is not due to measurement errors related to baseline or threshold settings.

The slow drift in the open stability plot is not due to obvious mode shifts

The fast Cl^- channel infrequently enters two kinetic gating modes other than normal: a buzz mode and an inactive shut state (Blatz & Magleby, 1986*a*). Since the inactive shut state involves single isolated shut intervals, it did not affect the open drift, as indicated by the apparent lack of correlation between entry into the inactive shut state and the slow open drift in Fig. 2*A* and *B*. To determine whether the buzz or other modes might contribute to the slow drift, high-resolution stability plots for

all data sets were constructed with five to fifty open or shut interval averaged for each mean (not shown). Such plots provide a sensitive method to detect different kinetic modes (Blatz & Magleby, 1986*a*; McManus & Magleby, 1988). Analysis of the high-resolution stability plots indicated that the slow drift is not due to obvious alternate kinetic modes.

Open and shut dwell-time distributions

Although stability plots provide a powerful tool to detect various types of kinetic modes, they have the limitation that any changes in gating that have little effect on the mean open or shut dwell times could go undetected. To overcome this limitation, we examined the stability of the dwell-time distributions of open and shut intervals throughout the experiment. Since the dwell-time distributions reflect the number of kinetic states and the transition rates among the states (Colquhoun & Hawkes, 1981), any changes in gating should alter the dwell-time distributions.

Figure 3 presents log–log plots of the open and shut dwell-time distributions for the 585000 intervals analysed for Fig. 2*A* and *B*, but with the five (inactive) shut intervals excluded. The continuous line in *A* is the best-fitted sum of two exponential components to the open distribution. The individual components are plotted as dashed lines. Two exponentials gave a significantly better fit of the open dwell times than one ($P < 0{\cdot}001$, likelihood ratio of 87·9) and three exponentials did not significantly improve the fit ($P > 0{\cdot}02$, likelihood ratio of 3·4). The continuous line in *B* is the best-fitted sum of six exponential components to the shut distribution. Six exponentials gave a significantly better fit of the shut distribution than five ($P < 0{\cdot}001$, likelihood ratio of 60·2) and seven exponentials did not significantly improve the fit ($P > 0{\cdot}1$, likelihood ratio of 2·3). Thus, these data are consistent with at least two open and six shut states during normal activity.

Table 2 lists the parameters of the exponential components describing the open and shut distributions. The time constants of the components are faster than those observed at a lower temperature by Blatz & Magleby (1986*a*), and there are six shut components compared to five. The detection of an additional shut component may reflect the sevenfold greater number of intervals analysed in the present study (e.g. McManus & Magleby, 1988).

Stability of dwell-time distributions

Figure 4 shows the stability of channel kinetics throughout the experiment. The 585000 intervals used for Figs 2 and 3 (inactive shut states excluded) were first divided into eleven consecutive subsets, each containing 25000 open and 25000 shut intervals. The continuous lines in Fig. 4 are the best-fitted sums of exponentials to each of the eleven open (*A*) and shut (*B*) distributions. There were still two open components, as observed in Fig. 3 when fitting all the intervals, but only five significant shut components, instead of six. The slowest shut component, with an area of only 0·00027 (Table 2), was too small to detect in the subsets of data.

Although the distributions remained remarkably consistent throughout the entire experiment, there were some differences. For example, the fastest shut component varied, as evident by the projection of the fits, and the shut distributions in the second and fourth subsets had more events at about 10 ms than the others.

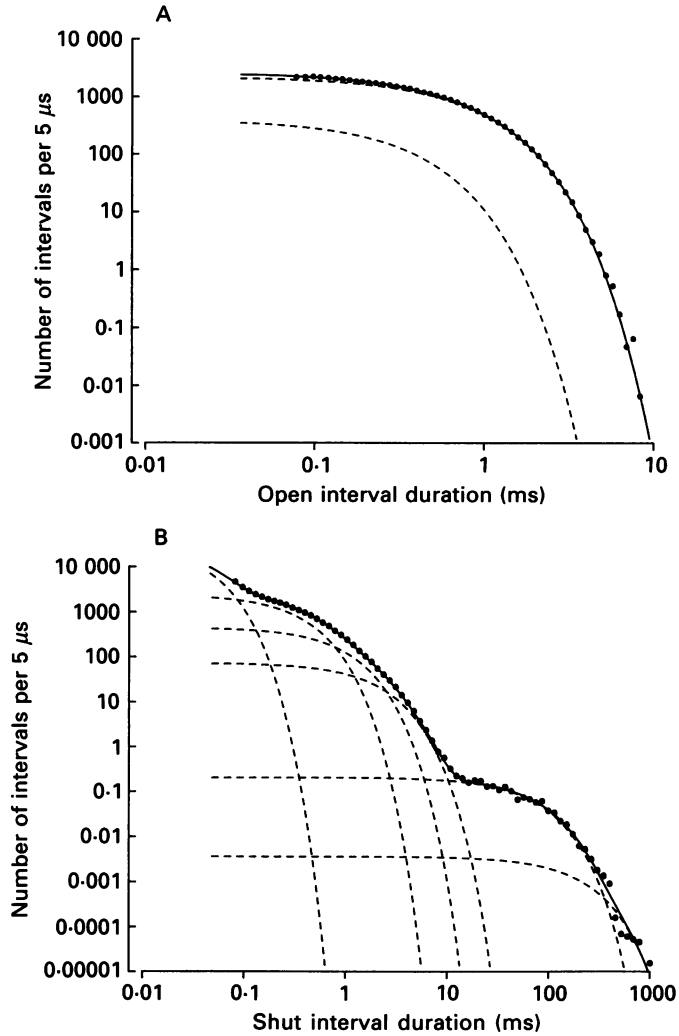

Fig. 3. Distributions of open and shut dwell-times at −40 mV. The durations of the intervals analysed for the open and shut stability plots in Fig. 2*A* and *B* were binned into frequency histograms and plotted on log–log co-ordinates (●). The continuous lines are the maximum likelihood fitted sums of two exponential components for the open distribution in *A* and of six exponential components for the shut distribution in *B*. The individual components are indicated by the dashed lines, and their areas and time constants are in Table 2. The distributions were fitted starting at 72·6 μs (about twice the dead time), and the five inactive shut intervals were excluded: 274441 intervals were fitted for the open distribution and 214994 for the shut. Intervals with durations less than two times the dead time were not plotted in the dwell-time distributions in this or subsequent figures.

Expected variability of the open and shut dwell-time distributions

Simulation was used to investigate whether the differences in the individual distributions in Fig. 4 arose from stochastic variation or drift in the underlying

gating. The expected stochastic variation was determined by analysing the intervals generated for the simulated stability plots in Fig. 2*C* and *D*. Figure 5 plots the means and standard deviations of the time constants and areas of the exponential components determined by individually fitting the eleven open and eleven shut distributions for both the experimental data (open bars) and simulated data (filled bars). Results for the two open components are in *A* and *B* and for the five shut components in *C* and *D*. The means and standard deviations for the experimental and simulated data appear similar. The similarity in the standard deviations suggest that the stochastic variation in the gating process together with any uncertainty in fitting are the major source of the variability in the experimental data. These findings argue against the possibility that an appreciable amount of the variability in the experimental data arises from baseline drift, or from alternate gating modes too subtle to detect in the stability plots, as these two types of errors would not be

TABLE 2. Parameters describing the distributions of open and shut interval durations at −40 mV

	Open		Shut	
Component	τ (ms)	Area	τ (ms)	Area
1	0·28	0·072	0·029	0·457
2	0·66	0·928	0·29	0·322
3	—	—	0·77	0·158
4	—	—	1·71	0·057
5	—	—	57·4	0·0054
6	—	—	163·7	0·00027

present in the simulated data. The results in this section do not account for the slow drift observed in Fig. 2, but suggest that it would have little effect on an analysis of voltage dependence.

P_{open} increases with depolarization

The single-channel records in Fig. 1 show that depolarization increases P_{open}. Figure 6*A* plots P_{open} *versus* membrane potential for the five fast Cl^- channels. The filled circles are from channel 1, the same channel presented in Figs 1–5 and the representative channel for the remainder of the paper. For channel 1 depolarization increased P_{open} from 0·038 at −90 mV to 0·56 at −20 mV, a 15-fold increase.

The slopes of the P_{open} plots are somewhat similar for the five channels, but some of the curves are shifted along the voltage axis. The two plots on the left were obtained at 23 °C and the two on the right at 18 °C. Temperature thus seems a likely cause for the shift, except the plot in the middle was also obtained at the higher temperature, suggesting possible kinetic heterogeneity.

Figure 6*B* shows fits of a Boltzmann distribution to the P_{open} *versus* membrane potential plots for channels 1 and 5. The equation used for the Boltzmann distribution assumes a two-state (open–shut) model for the gating and is described by (e.g. Hodgkin & Huxley, 1952; Hille, 1984):

$$P_{open} = 1/[1+\exp(-q(V-V_{0.5})/kT)], \quad (4)$$

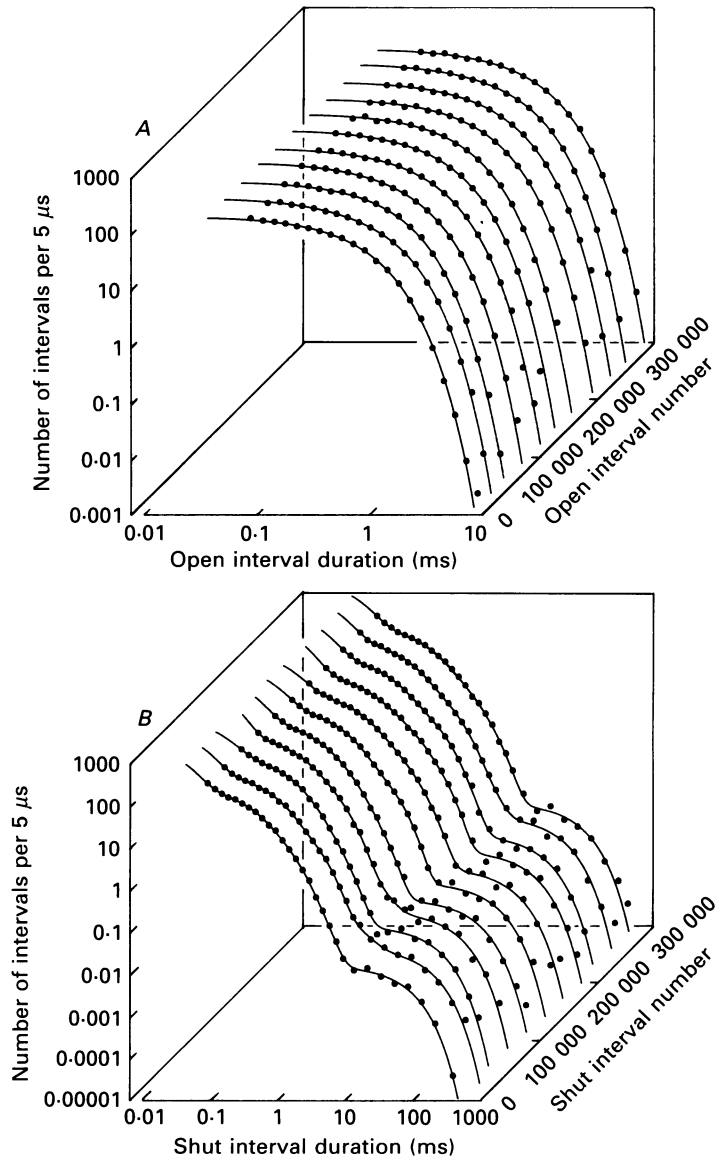

Fig. 4. Testing for kinetic stability with consecutive dwell-time distributions. The 585000 intervals collected at −40 mV and analysed for Figs 2 and 3 were divided into eleven consecutive groups of 50000 intervals, binned into frequency histograms, and plotted on log–log co-ordinates (●). The open dwell-time distributions in *A* were fitted (maximum likelihood) with the sums of two exponential components and the shut dwell-time distributions in *B* with five (continuous lines).

where q is the effective gating charge, $V_{0.5}$ is the voltage at which P_{open} is 0·5, k is the Boltzmann constant, and T is absolute temperature. The effective gating charge q is determined by the valency (z) of the moved charge times the value of an electronic charge ($e = 1{\cdot}6 \times 10^{-19}$ C) times the fractional distance (d) the charge moves in the electric field of the membrane; $q = zed$.

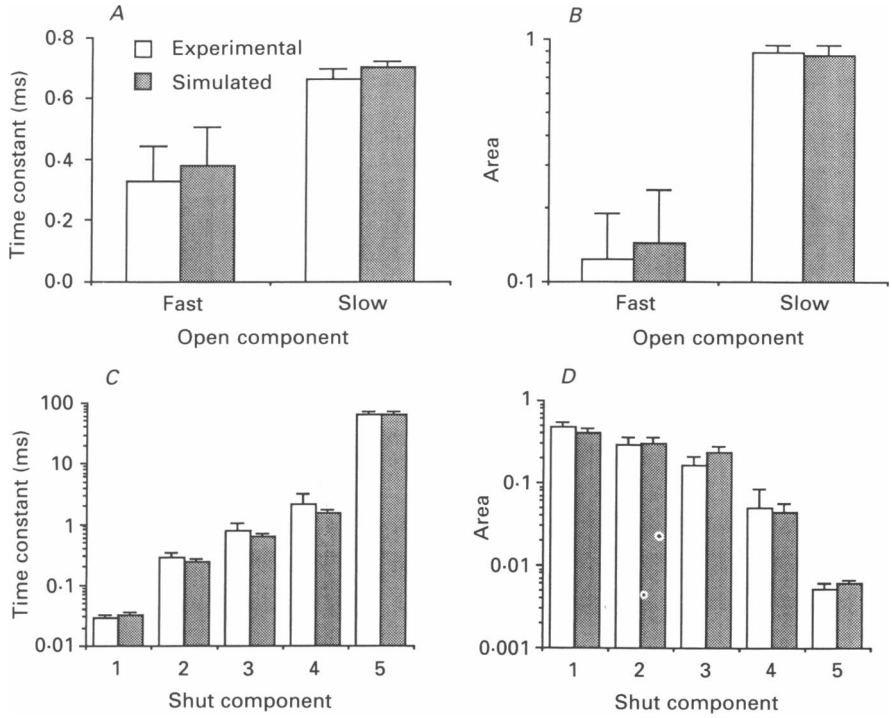

Fig. 5. The variability in the consecutive dwell-time distributions arises mainly from stochastic variation. *A* and *B*, plot of experimental and simulated means and standard deviations of the time constants and areas describing the two exponential components fitted to the eleven consecutive open time distributions in Fig. 4*A* and to eleven consecutive simulated open time distributions. Each of the experimental and simulated distributions contained 25000 intervals. The simulated data were generated using scheme I with state C_8 excluded and the rate constants listed in the legend of Fig. 2. *C* and *D*, experimental and simulated means and standard deviations of the five exponential components fitted to the eleven consecutive shut time distributions in Fig. 4*B* and to eleven consecutive simulated shut distributions.

Although the Boltzmann distribution approximates the P_{open} plots in Fig. 6*B*, there is a systematic error between the data points and the predicted distributions. The Boltzmann distribution tends to overestimate P_{open} at both hyperpolarized and depolarized potentials, and underestimates P_{open} at intermediate voltages. That the Boltzmann distribution cannot fully account for the data indicates that the gating of the fast Cl^- channel is more complicated than the simple two-state model assumed by eqn (4). This conclusion is consistent with the conclusion drawn from dwell-time distributions, that the fast Cl^- channel has multiple open and shut states (Table 2 and Blatz & Magleby, 1986*a*). A combination of two or more Boltzmann functions gave better fits to the data in Fig. 6*B* (not shown), but the limited number of data points were insufficient to adequately define the parameters.

The approximation of the data by a single Boltzmann distribution does, however, provide a means to compare the voltage sensitivity of the five examined channels through comparison of the fitted parameters q and $V_{0.5}$. Results are shown in Table 3. Also presented in Table 3 are estimates of q obtained from fitting a linear

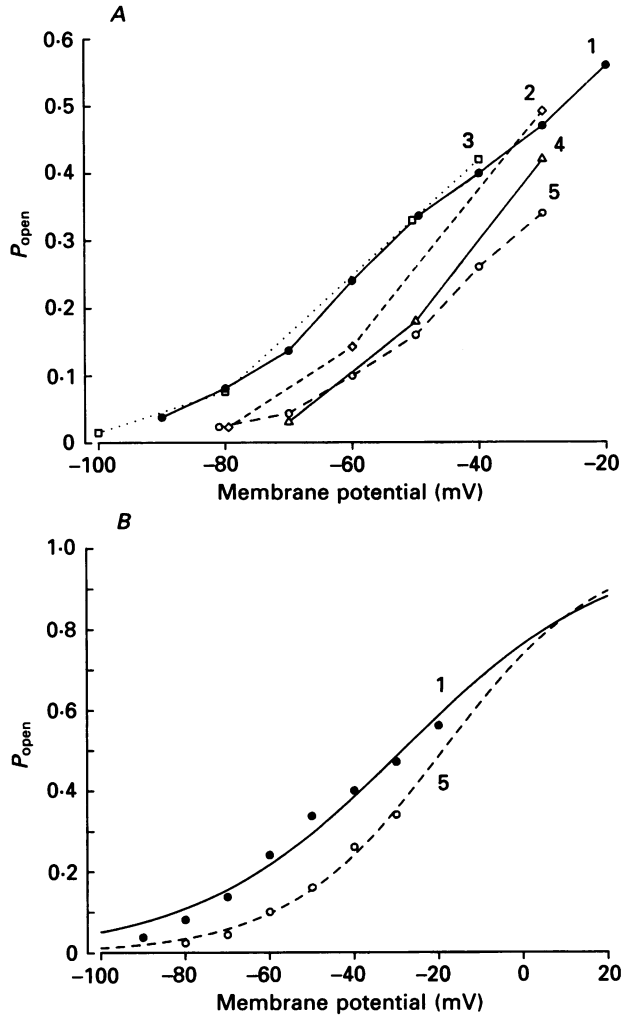

Fig. 6. Depolarization increases P_{open}. Plots of the fraction of time spent open, P_{open}, *versus* membrane potential. *A*, data for five separate fast Cl^- channels, numbered from 1 to 5 for identification with results in later figures. Channels 1–3 at 23 °C; channels 4–5 at 18 °C. *B*, a Boltzmann distribution only approximates the P_{open} data. The lines are least-squares fits with eqn (4) to the data from channels 1 and 5. Table 3 gives the values of q (in parentheses) and $V_{0.5}$.

regression to the logarithm of $P_{open}/(1-P_{open})$ *versus* membrane potential, a transform of the Boltzmann distribution. The two estimates of q differ because the errors are weighted differently in the fitting process.

Estimates of q varied somewhat, but were little affected by temperature, having a mean value of $1{\cdot}6 \pm 0{\cdot}3$ units of electronic charge at 23 °C (channels 1–3) and $1{\cdot}8 \pm 0{\cdot}3$ units at 18 °C (channels 4 and 5). The voltage at which the channel was open 50% of the time, $V_{0.5}$, was -31 ± 3 mV at 23 °C, and was shifted 9 mV in the depolarizing direction to -22 ± 5 mV for the 5 °C decrease in temperature.

For positive values of q and for V sufficiently large and negative, eqn (4) gives (e.g. Hodgkin & Huxley, 1952; Hille, 1984):

$$P_{open} = B \exp(qV/kT), \quad (5)$$

where B is a constant. An e-fold change in P_{open} occurs for each unit increase in qV/kT. Thus, the voltage sensitivity of the channel, expressed as the change in membrane potential required for an e-fold change in P_{open}, can be calculated from q with

$$\text{mV/e-fold change} = kT/q, \quad (6)$$

where kT equals 25·6 mV × electronic charge at 23 °C. Table 3 lists the calculated voltage sensitivity for the five channels. At 23 °C the mean voltage sensitivity was 17 ± 4 mV for an e-fold increase in P_{open}.

TABLE 3. Voltage sensitivity of five fast Cl^- channels

Channel	q	$V_{0.5}$	mV/ e-fold change
1	1·24 (1·04)	−28·5	20·6
2	1·86 (1·59)	−29·6	13·7
3	1·63 (1·37)	−35·1	15·6
4	1·95 (1·64)	−25·2	12·8
5	1·56 (1·36)	−18·9	16·0

$V_{0.5}$ is the potential for 50% of the time spent open, q is the effective gating charge, and mV/e-fold change is the voltage change necessary for an e-fold increase in P_{open}. Data for channels 1–3 were collected at 23 °C; data for channels 4 and 5 at 18 °C. Estimates of q in parentheses and $V_{0.5}$ were obtained by fitting eqn (4) to the data as in Fig. 6*B*. Estimates of q not in parentheses were calculated by linear regression to the logarithm of $P_{open}/(1-P_{open})$; mV/e-fold change was then calculated from these values of q with eqn (6).

Depolarization decreases mean shut time and increases mean open time

The current records in Fig. 1 show a depolarization-dependent decrease in the durations of shut intervals between and within bursts of openings. This effect of voltage on shut time is shown in Fig. 7 where the filled circles plot the mean shut interval duration as a function of voltage on semilogarithmic co-ordinates. The continuous line is a linear regression to the logarithm of the mean shut times calculated with

$$Y = Be^{AV}, \quad (7)$$

where Y is the mean shut time (or mean value of other parameters examined in later sections), V is the membrane potential, B is a constant, and A gives a measure of voltage sensitivity, expressed as the fractional change in Y per millivolt change in membrane potential. (Rather than reporting values of B, which specify Y at 0 mV and would be outside the range of the examined voltages, values of Y at −50 mV will be reported.) The mean shut time decreased e-fold for every 25·6 mV depolarization ($A = 0{\cdot}0391$ mV^{-1}), giving an effective gating charge of 1·0, calculated from eqn (6).

Fitting eqn (7) to the mean open times in Fig. 7 shows a moderate voltage dependence (○---○). The mean open time increased e-fold per 108 mV of

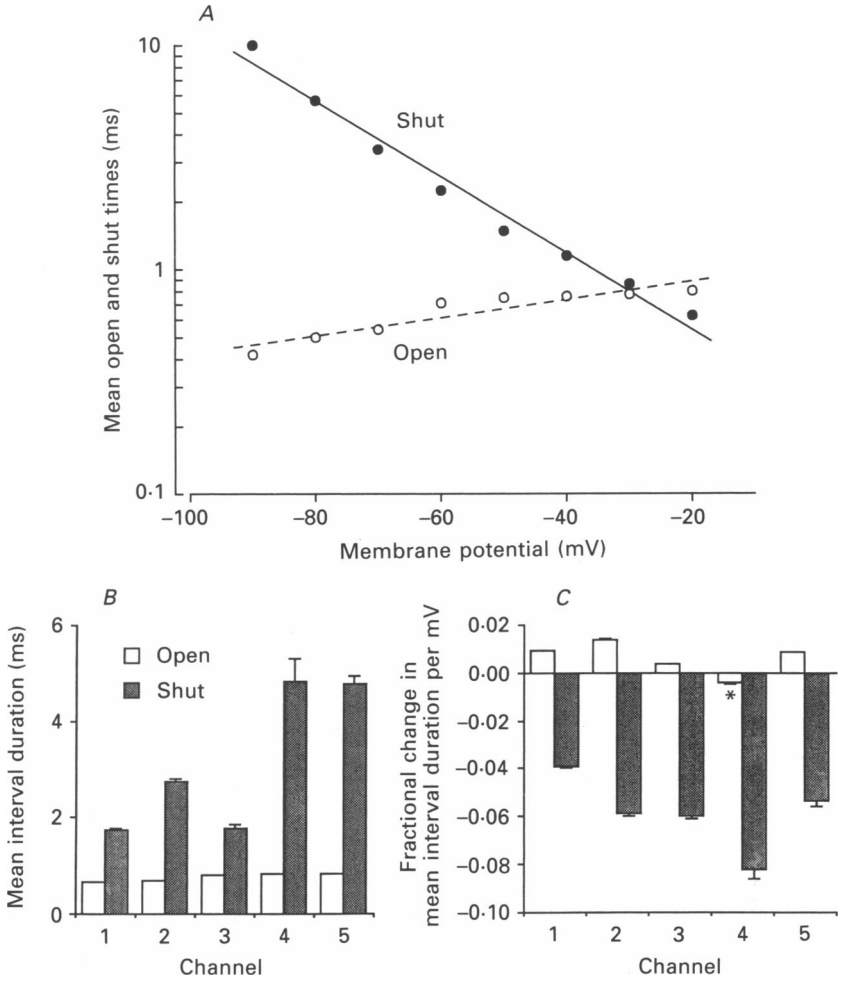

Fig. 7. Depolarization decreases mean shut time and increases mean open time. *A*, plot of mean open and mean shut times against membrane potential. The lines are a linear regression to the logarithm of the data (eqn (7)). *B*, mean open and shut times at −50 mV for the five channels. Plotted means are the values of *Y* at −50 mV, determined with eqn (7), as shown in panel *A*. *C*, voltage sensitivity of mean open and mean shut time for five channels, as defined by the value of *A* in eqn (7). Mean shut times decreased with depolarization for all five channels. Mean open times increased with depolarization for all channels except channel 4. The error bars were determined by resampling (see Methods).

depolarization ($A = 0{\cdot}0093\ \mathrm{mV}^{-1}$), yielding an effective gating charge of −0·23. The net effective charge for channel gating for the data in Fig. 7 would then be the combined effective gating charge for both channel closing and channel opening (1·00−(−0·23)), or 1·23. This value agrees with the effective gating charge of 1·24 determined from a linear regression to the logarithm of $P_{open}/(1-P_{open})$ *versus* membrane potential for this same channel (channel 1, Table 3).

The voltage dependence of the mean open and shut times for the other fast Cl^- channels was determined using the same analysis as in Fig. 7*A*. For the three

channels studied at 23 °C the voltage dependence of the decrease in mean shut time with depolarization was 19 ± 4 mV per e-fold change (effective gating charge of $1{\cdot}3 \pm 0{\cdot}3$), and the voltage dependence of the increase in mean open time with depolarization was 109 ± 61 mV per e-fold change (effective gating charge of $-0{\cdot}24 \pm 0{\cdot}13$).

The mean open and shut times at -50 mV (eqn (7)) are presented in Fig. 7*B*. The mean open times were similar for the five channels. The differences in the mean shut times were greater, with channels 1–3 (studied at 23 °C) having briefer shut times than channels 4 and 5 (studied at 18 °C).

The voltage sensitivities of the mean open and shut times for the five channels are presented in Fig. 7*C*. For all five channels depolarization decreased mean shut time. Interestingly, the direction of the voltage dependence of the mean open time was not the same for all channels. Depolarization increased mean open time for four of the channels and decreased mean open time for channel 4 (asterisk). Nevertheless, in all cases, the predominant effect of voltage on P_{open} was through its effect on mean shut time.

To determine whether the apparent differences among the parameters for the different channels in Fig. 7*B* and *C* could arise from limitations associated with a limited number of analysed interval and fitting errors, resampling was used (see Methods). The original data sets at each voltage for each channel were resampled and refitted with linear regression to the logarithm of the mean dwell-times, as in Fig. 7*A*. This entire procedure was repeated five times to obtain the plotted standard deviations. The standard deviations averaged only 2·4% of the plotted means, and in most cases are not visible. Thus, the observed differences in the parameters for the different channels in Fig. 7*B* and *C* are not due to errors associated with limitations in the number of analysed intervals or fitting.

Voltage does not alter the number of open and shut states

The data in Fig. 3 and Table 2 suggest that the fast Cl^- channel enters at least two open and six shut states during normal activity at -40 mV. Although voltage is unlikely to change the number of potential states, as this would imply an infinite gating charge for at least one of the transition pathways, it is possible that voltage could alter the rates sufficiently so that the detected number of states changes with membrane potential. For example, some states may become so infrequently entered at certain voltages that they would no longer contribute significantly to gating. (Changes in the effective numbers of states has previously been observed for some mode shifts (Blatz & Magleby, 1986*a*; McManus & Magleby, 1988).)

To investigate this possibility we examined the effect of membrane potential on the number of exponential components in the dwell-time distributions. A change in the number of components would be consistent with a change in the number of detected states (Colquhoun & Hawkes, 1981). Results are presented in Fig. 8 where each symbol plots results for a different channel. The number of detected exponential components remained relatively constant over the wide range of P_{open} (Fig. 6) associated with the examined range of membrane potentials (-100 to -30 mV), and in the few cases when a third open or seventh shut component was detected, the area of the component was small.

These findings suggest that membrane potential modulates channel activity

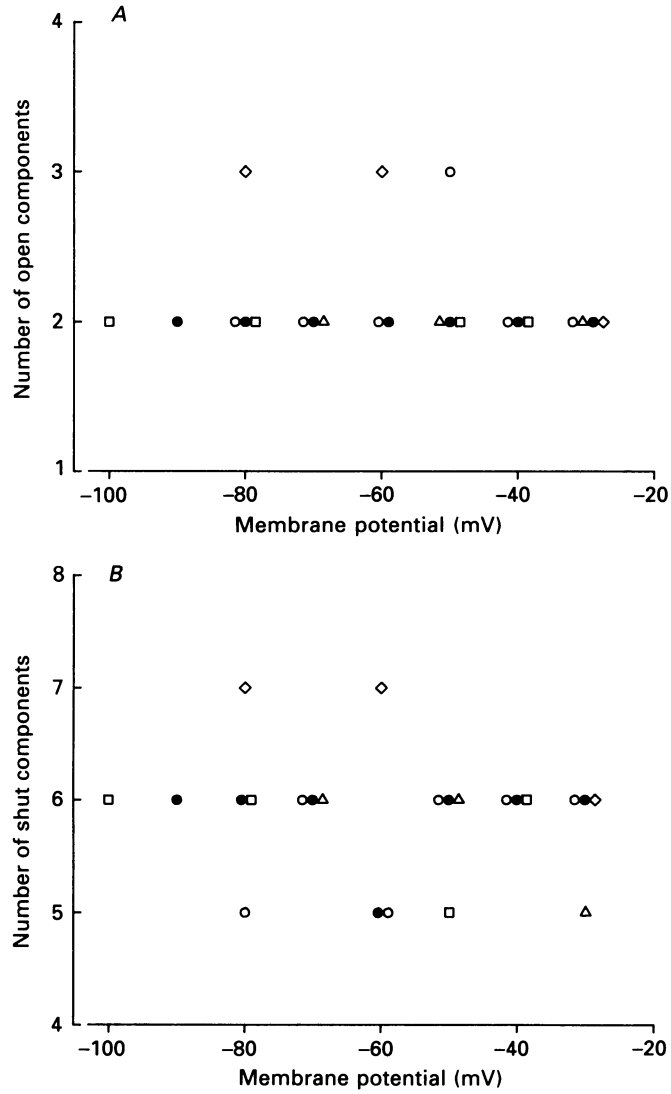

Fig. 8. The number of kinetic states appears independent of membrane potential. Open and shut dwell-time distributions were obtained at the indicated membrane potentials for the five channels. Each distribution was fitted with sums of exponentials to determine the number of significant components. The number of open exponential components are plotted against membrane potential in *A* and a similar plot is presented for the number of shut components in *B*. The channels typically enter at least two open and six shut states over the examined range of membrane potentials. The symbols designate the same channels as in Fig. 6*A*.

through changes in the dwell-times and frequency of entry into a relatively fixed collection of states. Examination of the effect of membrane potential on the parameters of the exponential components should give additional insight into the voltage-dependent changes.

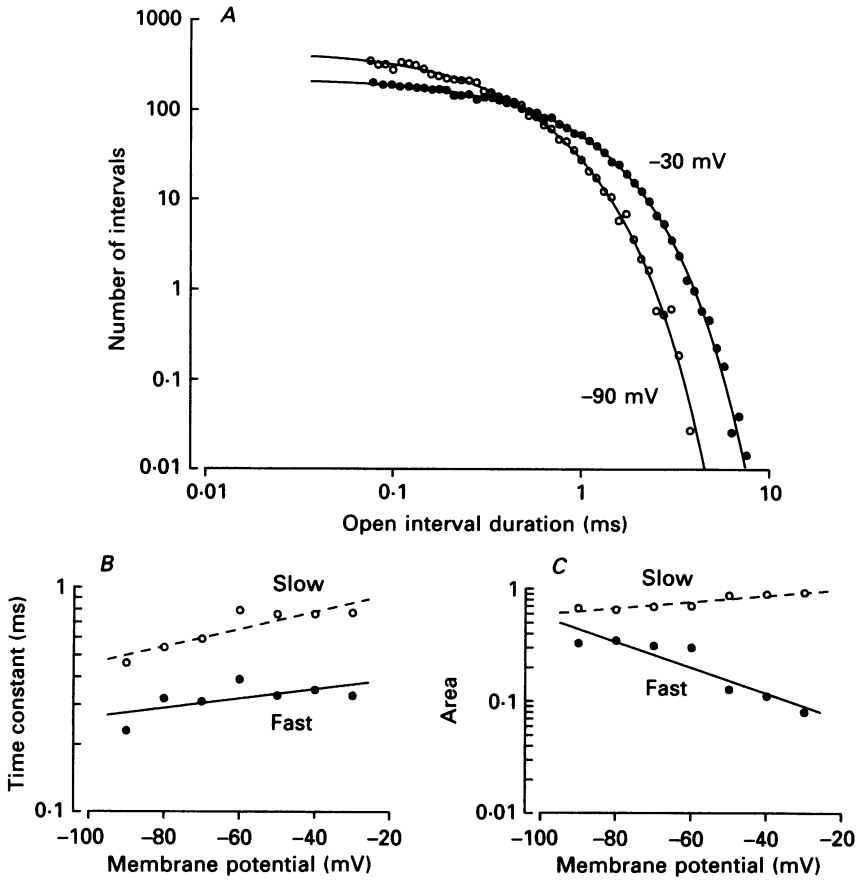

Fig. 9. Depolarization shifts the open dwell-time distributions towards longer open times. *A*, open dwell-time distributions obtained at −90 and −30 mV. The continuous lines are the maximum-likelihood fits to the data with the sums of two exponential components. The data at −90 mV were scaled so as to have the same number of intervals in the distribution as the data at −30 mV; 27258 intervals were fitted for the distribution at −30 mV and 6506 for the distribution at −90 mV. *B* and *C*, the effect of voltage on the exponential components describing the open dwell-time distributions. The time constants (*B*) and areas (*C*) of the fast and slow components are plotted against membrane potential. The values at −90 and −30 mV were obtained from the data in *A*. The lines are a linear regression to the logarithm of the data (eqn (7)).

Effect of voltage on the distribution of open times

Figure 9 plots distribution of open dwell times at −90 mV (○) and −30 mV (●). Depolarization decreased the relative proportion of brief events and increased the relative proportion of longer events. Distributions at intermediate voltages fell between the two plotted distributions. The shift in the distributions with voltage is characterized in Fig. 9*B* and *C*, which presents semilogarithmic plots of the time constants and areas of the fast and slow open components at seven different voltages. The lines are linear regressions to the logarithm of the values with eqn (7). Depolarization increased the time constants of both open components, with a voltage

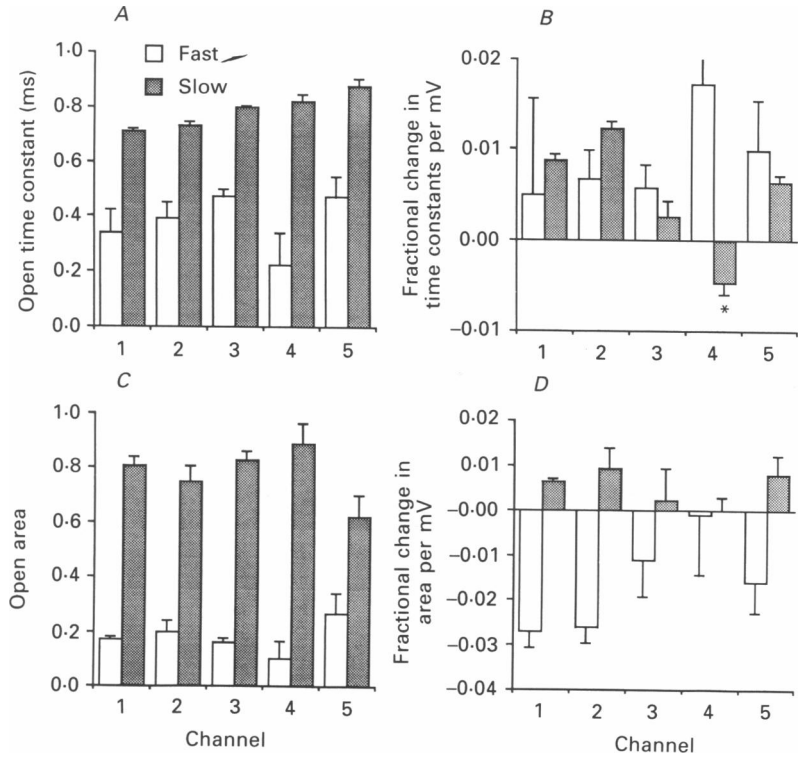

Fig. 10. Voltage-dependent changes in the open dwell-time distributions for the five channels. *A*, time constants at −50 mV for the fast (□) and slow (■) open exponential components. Plotted time constants are the values of *Y* at −50 mV, determined with eqn (7). *B*, voltage dependence of the time constants for the fast and slow open exponential components (*A* in eqn (7)). The fast and slow time constants increased with depolarization for all but channel 4, where the slow time constant decreased with depolarization (asterisk). *C*, areas at −50 mV (calculated with eqn (7)) for the fast and slow open exponential components. *D*, voltage dependence of the areas of the fast and slow components (*A* in eqn (7)). Depolarization decreases the area of the fast component and increases the area of the slow component for all channels except channel 4, where depolarization has little effect on the areas. The error bars were determined by resampling (see Methods).

sensitivity (*A* in eqn (7)) of 0·0049 mV^{-1} for the fast component and 0·0089 mV^{-1} for the slow component. The inverse of these *A* values gives 204 and 112 mV per e-fold increase in the time constant for the fast and slow components, respectively. Depolarization increased the area of the slow component ($A = 0{\cdot}00579\ mV^{-1}$) and decreased the area of the fast component ($A = -0{\cdot}0245\ mV^{-1}$).

Figure 10 summarizes the voltage dependence of the open distributions for all five channels. For each channel the open distributions at the various voltages were fitted with the sum of two exponentials, as shown in Fig. 9*B* and *C*. The values of the fast and slow time constants at −50 mV (calculated with eqn. (7)) and the voltage sensitivities of the time constants (*A* in eqn (7)) are plotted in Fig. 10*A* and *B*. The areas of the two components at −50 mV and their voltage sensitivities are plotted in Fig. 10*C* and *D*.

The components describing the open distributions were generally similar for the five channels. At −50 mV the time constant of the slow component was typically twice that of the fast component (Fig. 10*A*), and the area of the slow component was typically 80% compared to 20% for the fast component (Fig. 10*C*). The slightly larger values for the slow time constant for channels 4 and 5 when compared to channels 1–3 may reflect the 5 °C difference in temperature of the experiments. The error bars (determined by resampling) indicated that the larger value of the slow time constant for channel 3, when compared to channels 1 and 2, was greater than the expected errors arising from the limited number of intervals and fitting errors.

The voltage dependence of the parameters describing the open components (Fig. 10*B* and *D*) showed more variability than the parameters themselves. However, if channel 4 was excluded, the voltage dependence of the remaining channels was consistent; the time constants of both the fast and slow components increased with depolarization (positive voltage sensitivities in Fig. 10*B*), and the area of the fast component decreased while the area of the slow component increased with depolarization (negative and positive voltage sensitivities, respectively in Fig. 10*D*).

Channel 4 appears different from the other channels in that the voltage dependence of the slow open component decreases (asterisk, Fig. 10*B*), rather than increases, with depolarization. Furthermore, the areas of both the fast and slow components for channel 4 seem independent of voltage, in contrast to the other channels (Fig. 10*D*). The apparent reversed voltage sensitivity of the time constant of the slow open component of channel 4 could not be accounted for by uncertainty arising from the limited number of intervals and fitting errors, while the apparent lack of voltage sensitivity of the areas of the open components may simply reflect errors in the estimates, as indicated by the error bars. Channel 4 is the same channel noted as being different in Fig. 7*C*, where the mean open duration decreased, rather than increased, with depolarization. Thus, the depolarization-dependent decrease in the mean open duration of channel 4 is primarily due to a depolarization-dependent decrease in the time constant of the slower open component, which contains 82% of the open intervals at −50 mV.

Effect of voltage on the distribution of shut times

Figure 11 plots distributions of shut dwell times at −90 mV and −30 mV. Distributions at intermediate voltages fell between the two plotted distributions. The continuous lines are the best fits to the data with the sums of six exponential components. The depolarization of 60 mV shifted the distribution to the left so that the shut times were typically decreased by an order of magnitude. The fact that the entire distribution was shifted indicates that most of the time constants were made faster by depolarization. In addition to decreasing the time constants, depolarization also increased the relative proportion of briefer shut intervals.

This shift in the distributions with voltage is characterized in Fig. 11*B–G* which presents semilogarithmic plots of the time constants and areas for the six components *versus* voltage. The components are labelled from fastest (1) to slowest (6). For components 1–4, eqn (7) gave reasonable approximations of the voltage dependence of the parameters. There was, however, increased scatter about the lines for components 5 and 6 because of the limited numbers of intervals defining the two

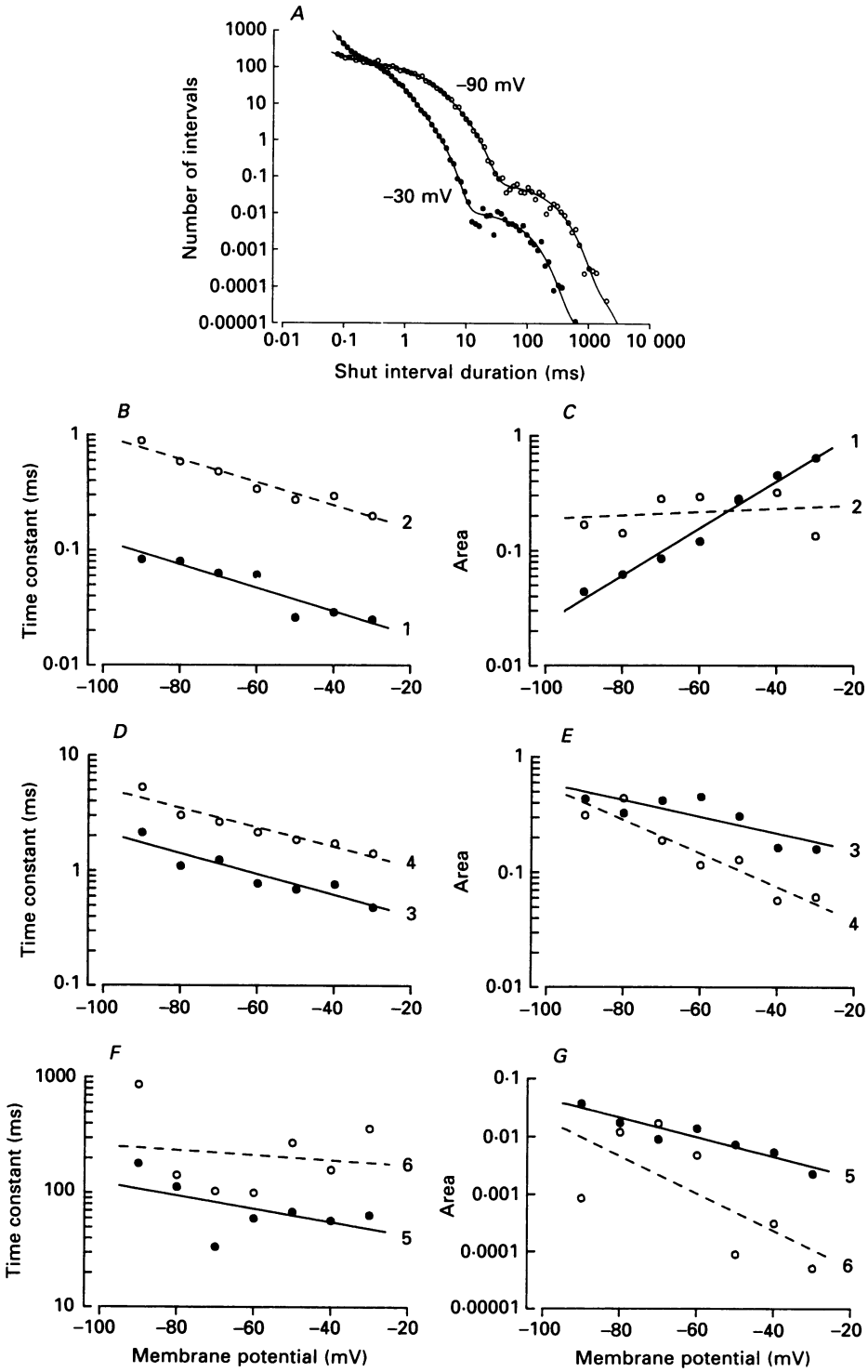

Fig. 11. For legend see facing page.

slowest components. Figure 11 shows that depolarization decreased the time constants of all six components and shifted net area from the four slower components to the fastest component, with little change in the area of the second fastest component. The observation at negative potentials that the fastest component no longer has the largest area is inconsistent with the diffusion gating model of Millhauser, Salpeter & Oswald (1988).

Figure 12 summarizes the effects of voltage on the areas and time constants of the components describing the shut time distributions for all five channels. The time constants of the exponential components were relatively consistent for all five channels (Fig. 12*A*), while there was more variability in the areas (Fig. 12*C*). Although the general form of the plotted data was the same for the five channels, resampling (see Methods) indicated that some of the differences were greater than the uncertainty due to a limited number of analysed intervals and fitting errors. For example, the time constants of the first three components of channel 4 were greater than those of channel 5, and the time constants of the first and fourth components of channel 1 were greater and less, respectively, than those of channel 3. The area of the fourth component of channel 1 was greater than for channels 2 and 3, and the area of the fifth component of channel 3 was less than that of channels 1 and 2.

The voltage dependence of the shut time constants is presented in Fig. 12*B*. For channels 1, 2 and 5 the time constants of all six components decreased with depolarization (negative voltage sensitivity). For channels 3 and 4 the time constants of the five slower components also decreased with depolarization, but the time constant of the fastest component increased. Resampling suggested that this apparent reversed voltage sensitivity of the fastest shut time constant was unlikely to arise from uncertainty due to limited sample size and fitting errors.

The voltage dependence of the areas of the shut components are presented in Fig. 12*D*. On average, the area of the fastest component increased with depolarization (positive voltage sensitivity), the areas of the four slower components decreased, and the area of the second fastest component was little changed. Resampling indicated that some of the differences in the voltage sensitivities of the areas, such as the difference between the fastest component of channels 4 and 5, would be unlikely to arise from uncertainty due to the limited number of analysed intervals and fitting errors.

Figures 11 and 12 show that depolarization decreases mean shut time in two ways: it generally decreases the duration of all the shut intervals (the time constants of the components decrease) and it shifts net area (closings) from the four components of longer duration to the component of briefest duration.

Fig. 11. Depolarization shifts the shut dwell-time distributions towards briefer shut times. *A*, shut dwell-time distributions obtained at −90 and −30 mV. The continuous lines are the maximum-likelihood fits to the data with the sums of six exponential components. The data at −90 mV were scaled so as to have the same number of intervals in the distribution as the data at −30 mV; 22049 intervals were fitted for the distribution at −30 mV and 6990 for the distribution at −90 mV. *B–G*, the effect of membrane potential on the time constants and areas of the six exponential components fitted to the shut dwell-time distributions. The components are numbered from fastest (1) to slowest (6). The lines are a linear regression to the logarithm of the data (eqn (7)).

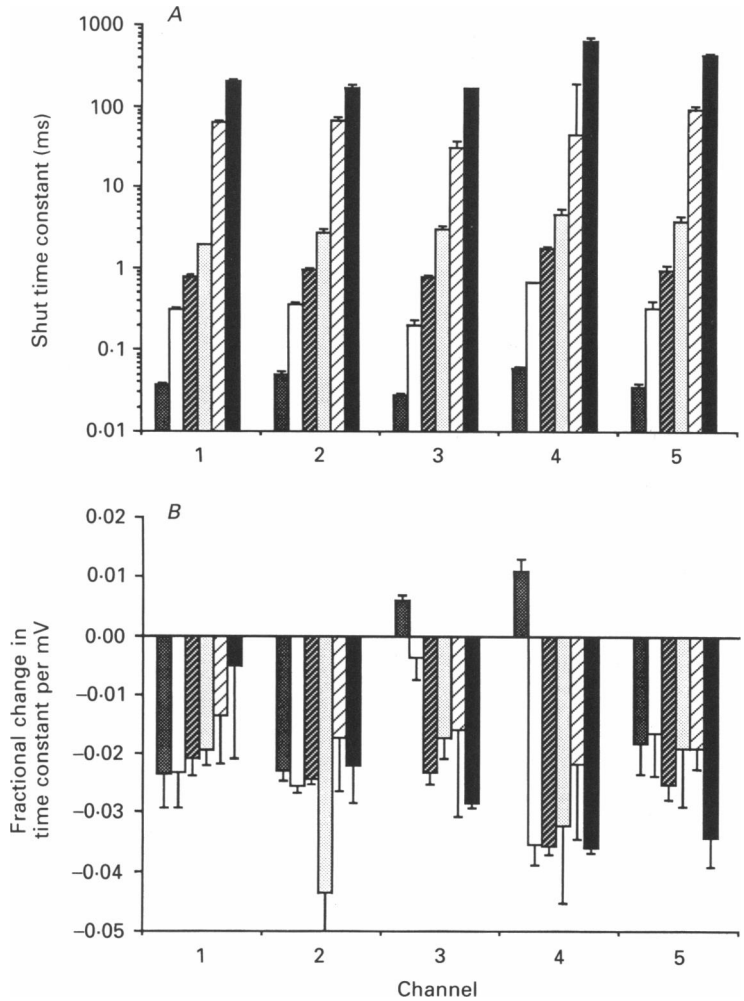

Fig. 12. Voltage-dependent changes in the shut dwell-time distributions for the five channels. The six bars for each channel indicate values for the six components. In each case, the bar on the left indicates the fastest component (component 1), with the five successive bars to the right indicating components 2–6. *A*, time constants at −50 mV for the six shut exponential components. Plotted time constants are the values of *Y* at −50 mV, determined with eqn (7). *B*, voltage dependence of the time constants for the

DISCUSSION

The study investigates the kinetic stability, voltage dependence, and kinetic heterogeneity of the fast Cl^- channel in cultured rat skeletal muscle. The primary observations are: (1) the gating kinetics of the fast Cl^- channel can remain reasonably stable over extended periods of time sufficient to collect over 10^6 intervals; (2) there are some heterogeneities in the voltage-dependent kinetics among the five examined fast Cl^- channels, but the differences are small compared to the similarities; (3) the voltage dependence of the gating kinetics are complex, in

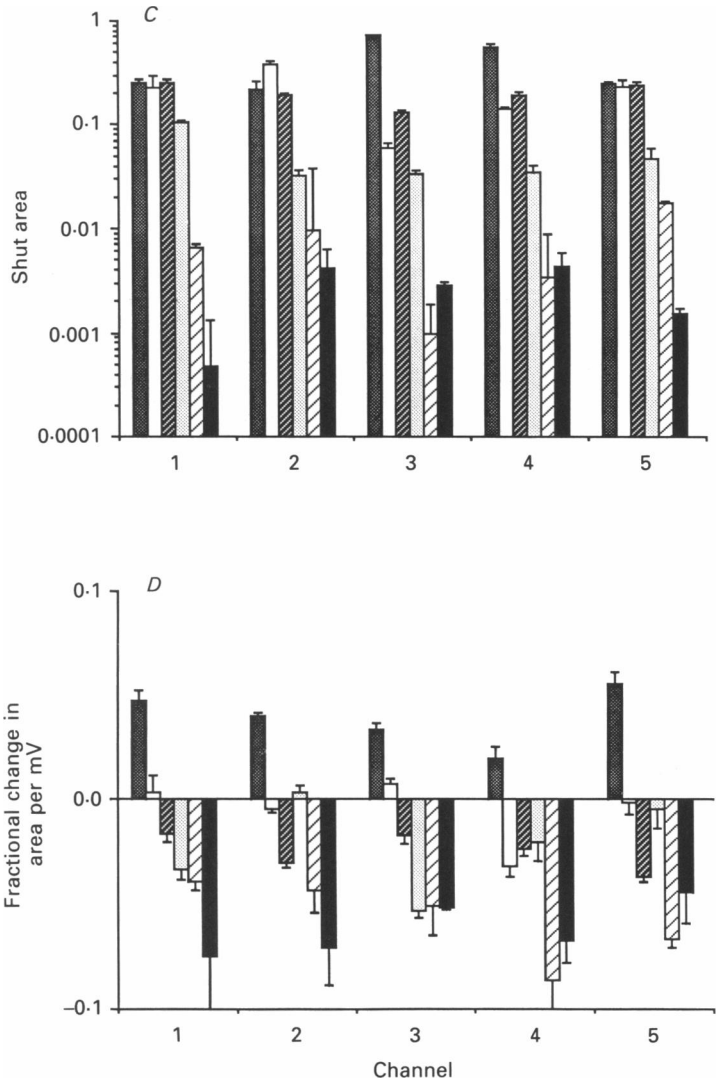

six shut components (A in eqn (7)). The time constants of all six components typically decreased with depolarization (negative voltage sensitivity). *C*, areas at −50 mV (calculated with eqn (7)) for the six exponential components. *D*, voltage dependence of the areas (A in eqn (7)). Depolarization typically increases the area of the fastest component, has little effect on the second fastest component, and decreases the area of the slower components. The error bars were determined by resampling (see Methods).

that depolarization typically acts to change most of the kinetic parameters in a manner to produce a smoothly graded increase in P_{open}.

Long-term stability of gating

Many ion channels change their kinetic properties over time by switching among different modes, and/or displaying marked heterogeneities in kinetics (Patlak *et al.* 1979; Moczydlowski & Latorre, 1983; Hess *et al.* 1984; Patlak & Ortiz, 1986; Patlak

et al. 1986; McManus & Magleby, 1988; Nilius, 1988; cf. Lacerda & Brown, 1989). The fast Cl^- channel also displays several different gating modes, with 99% of the intervals occurring during normal mode activity (Blatz & Magleby, 1986*a*). We have extended the analysis of the fast Cl^- channel to investigate long-term gating stability (25 min).

Stability plots of the mean open interval durations showed a slow drift of small magnitude which could not be accounted for by stochastic variation (Fig. 2, Table 1). This slow drift typically required in excess of 50000–100000 open intervals to observe. Repeated analysis of selected current records indicated that it was not due to measurement errors during event detection. Furthermore, the remarkable stability of the dwell-time distributions over time (Figs 4 and 5) indicated that the drift was not due to any obvious changes in the gating kinetics. Thus, the drift may arise from such small changes in the transition rates that the dwell-time distributions are not significantly altered.

Changes in membrane potential from electrode drift seem unlikely to be the major cause for the small changes in transition rates, since the 10% drift in mean open time (Fig. 2*A*) would require a 10 mV electrode drift (Fig. 7; 108 mV per e-fold change), far greater than might be expected to occur during a typical experiment. Another argument against electrode drift is that it would require that the drift in the mean open and shut times be inversely related because of their opposite voltage sensitivities (Fig. 7). A consistent inverse relationship was not observed (Fig. 2). Any changes in room temperature (typically stable to a few tenths of a degree during an experiment) also seem unlikely to be the major contributor to the drift, since temperature-induced drift might also be expected to alter open and shut times in a correlated manner. Whatever the underlying mechanism of the slow drift, any affects on the dwell-time distributions appear less than those from stochastic variation.

Kinetic heterogeneity among fast Cl^- channels

The five studied fast Cl^- channels were similar in that P_{open} increased with depolarization (Fig. 6). However, the plots of P_{open} *versus* voltage were different for the different channels, and detailed examination of the voltage-dependent kinetics revealed some additional differences (Figs 7, 10 and 12). Our ability to obtain large amounts of data from single-channel patches, and to restrict the analysis to normal mode activity, excludes the possibility that any of the kinetic differences might arise from mode shifts.

One of the more interesting differences was the observation that the mean open time decreased, rather than increased, with depolarization for channel 4 (Fig. 7*C*). Nevertheless, the P_{open} *versus* voltage curve for channel 4 was still similar to the other channels because of the overwhelming voltage sensitivity of the mean shut time (Fig. 7*C*).

The reversed voltage sensitivity of the mean open time for channel 4 could rise from a reversed voltage sensitivity of a rate constant associated with closing from one of the open states. Alternatively, a change in a rate constant leaving a shut state could lead indirectly to a change in observed open times through undetected shut events (e.g. Colquhoun & Sigworth, 1983). In support of this possibility, inspection of the components of the shut distributions in Fig. 12 indicates that the time constant

of the shut component with the briefest duration increased with depolarization for channel 4 (Fig. 12*B*), while typically decreasing for the other channels. Consequently, more shut events would be detected for channel 4, leading to a decrease in the observed open time. Whatever the underlying mechanism for the reversed voltage sensitivity of the open time for channel 4, the observation is sufficient to indicate that the kinetics of channel 4 differ from the other channels.

Kinetic heterogeneity in other channel types and possible mechanisms

Heterogeneity in the voltage dependence of channel opening has been observed for Na^+ channels inserted into bilayers (Hartshorne, Keller, Talvenheimo, Catterall & Montal, 1985). In this case, the heterogeneity was observed as a shift in the voltage at which P_{open} was 0·5, without a change in the effective gating charge. Heterogeneity in the kinetics of Na^+ channels has also been observed by Patlak *et al.* (1986) in frog muscle and Nilius (1988) in isolated ventricular cells of guinea-pig hearts. The open-time kinetics of bursting Na^+ channels could be markedly heterogeneous between different bursts, but were not so within a single burst. This bursting heterogeneity could arise from heterogeneity among channels or from mode shifts within channels (Patlak *et al.* 1986). In contrast to the pronounced heterogeneity for Na^+ channels, the heterogeneity we observed among fast Cl^- channels might best be thought of as micro-heterogeneity, since the kinetic differences were small and would be difficult to detect by visual observation of the current records.

Some potential mechanisms for kinetic heterogeneity have been considered previously (Hartshorne *et al.* 1985; Patlak *et al.* 1986; Nilius, 1988). Different genes (e.g. Butler, Wei, Baker & Salkoff, 1989) or alternate splicing (e.g. Schwarz, Tempel, Papazian, Jan & Jan, 1988) may yield channels with similar functions but different kinetic properties. Possible transcription or translation errors could also lead to an occasional channel with different kinetics. Differences in post-transcriptional modification, such as degree of glycosylation (e.g. James & Agnew, 1987) or phosphorylation (e.g. Novak-Hofer & Levitan, 1986) could also affect channel properties. Possible enzymatic degradation or an altered membrane environment due to contact with other proteins in the patch or contact with the patch pipette might also lead to kinetic differences and heterogeneity.

Voltage-dependent gating

The voltage sensitivity of the fast Cl^- channel was 17 ± 4 mV depolarization per e-fold increase in P_{open} at 23 °C (Fig. 6, Table 3), with the channel open 50% of the time at -31 ± 4 mV. This voltage sensitivity translates to $1{\cdot}6 \pm 0{\cdot}3$ effective gating charges, equivalent to the net transfer of 1·6 electronic charges across the entire field of the membrane for a channel to open and then close again, assuming a two-state model. For comparison, the effective gating charge of the dimeric Cl^- channel from electroplax is 1·1, with a 50% open probability at -85 mV (Hanke & Miller, 1983). The effective gating charge of the batrachotoxin-modified Na^+ channel is 3·9 in rat brain (Keller, Hartshorne, Talvenheimo, Catterall & Montal, 1986) and 5·4 in squid optic lobe (Behrens, Oberhauser, Bezanilla & Latorre, 1989), and the effective gating charge of the delayed rectifier K^+ channel is 7 in squid axon (White & Bezanilla, 1985). In contrast, the effective gating charge of the GABA-gated channel and the

decay of the endplate current are only 0·3 (Weiss, 1988) and −0·23 (Magleby & Stevens, 1972), respectively. Thus, the voltage dependence of the fast Cl^- channel in cultured skeletal muscle is similar to that of the dimeric Cl^- channel, but is 3–5 times less voltage dependent than the Na^+ and K^+ channels which underlie the action potential, and 4–5 times more voltage dependent than two agonist-activated, voltage-modulated channels.

The fast Cl^- channel appears ideally designed to yield a smoothly graded increase in P_{open} with depolarization. (In considering possible mechanisms for this increase, the atypical result for channel 4 will be excluded.) Depolarization decreases the time constants of all six shut components (Fig. 12*A* and *B*) and shifts net area (closings) from the four slower components to the fastest (Fig. 12*C* and *D*). Depolarization has just the opposite effect on the open components, increasing the time constants of both open components (Fig. 10*B*) and shifting the area (openings) from the faster component to the slower (Fig. 10*C* and *D*). Thus, depolarization changes most of the components of the open and shut distributions, and all these changes act to increase P_{open}.

A working hypothesis for the gating of the fast Cl^- channel during normal activity at −40 mV has been proposed by Blatz & Magleby (1986*a*, 1989), and is given by scheme I, where O and C represent open and closed states. The lifetimes of the shut states decrease from left to right, and the effective lifetime of O_1 is greater than that of O_2. (We have added an additional shut state to be consistent with our results.)

$$\begin{array}{ccccccccccc} C_8 & \rightleftharpoons & C_7 & \rightleftharpoons & C_6 & \rightleftharpoons & C_5 & \rightleftharpoons & C_4 & \rightleftharpoons & C_3 \\ & & & & & & & & \uparrow\downarrow & & \uparrow\downarrow \\ & & & & & & & & O_2 & & O_1 \end{array} \qquad \text{(I)}$$

The observation that a Boltzmann distribution only approximated the effect of voltage on P_{open} (Fig. 6*B*) and on the mean open and shut times (Fig. 7*A*) suggests that a number of the transition rates in scheme I are voltage dependent. The further observation that changes in membrane potential sufficient to change P_{open} 10- to 15-fold had little effect on the number of detected exponential components (Fig. 8), but gave progressive changes in the areas and time constants of the components, suggests that voltage does not change any of the rates sufficiently to either prevent entry into any of the states or reveal a new state.

In terms of scheme I, the voltage dependence of the open and shut dwell-time distributions results from a voltage-dependent shift towards the right in the equilibrium occupancy of the open and shut states. This shift would decrease the number of long shut intervals involving one or more of the states C_8 through C_5 and increase the number of brief shut intervals mainly involving state C_3. A shift to the right would also decrease openings to the briefer open state O_2, and increase openings to the longer open state O_1. The observed increase in the time constants of the two open components with depolarization (Figs 9 and 10) could arise from a depolarization-induced slowing of the rate constants away from O_1 and O_2. Alternatively, the observed increase in the open time constants could arise from the depolarization-induced decrease in the durations of shut intervals (Fig. 12). Fewer shut intervals would be detected, leading to an increase in the observed open times.

The next step will be to determine the voltage sensitivity of the various rate constants in scheme I so that a quantitative test of the above working hypothesis for the voltage dependence of the fast Cl^- channel can be carried out.

We thank Dr W. Nonner for helpful discussions. This work was supported by fellowships from the NIH to D.S.W. (NS 08138 and NS 07044) and grants from the NIH (AR 32805) and Muscular Dystrophy Association to K.L.M.

REFERENCES

ALDRICH, R. W., COREY, D. P. & STEVENS, C. F. (1983). A reinterpretation of mammalian gating based on single channel recording. *Nature* **306**, 436–441.

ARMSTRONG, C. M. & BEZANILLA, F. (1977). Inactivation of the sodium channel. *Journal of General Physiology* **70**, 567–590.

BARRETT, J. N., BARRETT, E. F. & DRIBIN, L. B. (1981). Calcium-dependent slow potassium conductance in rat skeletal myotubes. *Developmental Biology* **82**, 258–266.

BARRETT, J. N., MAGLEBY, K. L. & PALLOTTA, B. S. (1982). Properties of single calcium-activated potassium channels in cultured rat muscle. *Journal of Physiology* **331**, 211–230.

BEHRENS, M. I., OBERHAUSER, A., BEZANILLA, F. & LATORRE, R. (1989). Batrachotoxin-modified sodium channels from squid optic nerve in planar bilayers. Ion conduction and gating properties. *Journal of General Physiology* **93**, 23–41.

BLATZ, A. L. & MAGLEBY, K. L. (1985). Single chloride-selective channels active at resting membrane potentials in cultured rat skeletal muscle. *Biophysical Journal* **47**, 119–123.

BLATZ, A. L. & MAGLEBY, K. L. (1986*a*). Quantitative description of three modes of activity of fast chloride channels from rat skeletal muscle. *Journal of Physiology* **378**, 141–174.

BLATZ, A. L. & MAGLEBY, K. L. (1986*b*). Correcting single-channel data for missed events. *Biophysical Journal* **49**, 967–980.

BLATZ, A. L. & MAGLEBY, K. L. (1987). Calcium-activated potassium channels. *Trends in Neurosciences* **10**, 463–467.

BLATZ, A. L. & MAGLEBY, K. L. (1989). Adjacent interval analysis distinguishes among gating mechanisms for the fast chloride channel from rat skeletal muscle. *Journal of Physiology* **410**, 561–585.

BUTLER, A., WEI, A., BAKER, K. & SALKOFF, L. (1989). A family of putative potassium channel genes in *Drosophila*. *Science* **243**, 943–947.

COLQUHOUN, D. (1988). Single-channel analysis costs time. *Trends in Pharmacological Sciences* **9**, 157–158.

COLQUHOUN, D. & HAWKES, A. G. (1981). On the stochastic properties of single ion channels. *Proceedings of the Royal Society* B **211**, 205–235.

COLQUHOUN, D. & SIGWORTH, F. J. (1983). Fitting and statistical analysis of single-channel records. In *Single-Channel Recording*, ed. SAKMANN, B. & NEHER, E., pp. 191–263. Plenum Press, New York.

EFRON, B. (1982). *The Jackknife, the Bootstrap, and Other Resampling Plans*. Society for Industrial and Applied Mathematics, Philadelphia.

HAMILL, O. P., MARTY, A., NEHER, E., SAKMANN, B. & SIGWORTH, F. J. (1981). Improved patch-clamp techniques for high-resolution current recording from cells and cell-free membrane patches. *Pflügers Archiv* **391**, 85–100.

HANKE, W. & MILLER, C. (1983). Single chloride channels from *Torpedo* electroplax: activation by protons. *Journal of General Physiology* **82**, 23–45.

HARTSHORNE, R. P., KELLER, B. U., TALVENHEIMO, J. A., CATTERALL, W. A. & MONTAL, M. (1985). Functional reconstitution of the purified brain sodium channel in planar lipid bilayers. *Proceedings of the National Academy of Sciences of the USA* **82**, 240–244.

HESS, P., LANSMAN, J. B. & TSIEN, R. W. (1984). Different modes of Ca^{2+} channel gating behaviour favoured by dihydropyridine Ca^{2+} agonists and antagonists. *Nature* **311**, 538–544.

HILLE, B. (1984). *Ionic Channels of Excitable Membranes*. Sinauer Associates Inc., Sunderland, MA, USA.

HODGKIN, A. L. & HUXLEY, A. F. (1952). A quantitative description of membrane current and its application to conduction and excitation in nerve. *Journal of Physiology* **117**, 500–544.

HORN, R. (1987). Statistical methods for model discrimination: application to gating kinetics and permeation of the acetylcholine receptor channel. *Biophysical Journal* **51**, 255–263.

HORN, R. & LANGE, K. (1983). Estimating kinetic constants from single channel data. *Biophysical Journal* **43**, 207–223.

HORN, R. & VANDENBERG, C. A. (1984). Statistical properties of single sodium channels. *Journal of General Physiology* **84**, 505–534.

JAMES, W. M. & AGNEW, W. S. (1987). Multiple oligosaccharide chains in the voltage-sensitive Na channel from *Electrophorus electricus*: evidence for alpha-2,8,-linked polysialic acid. *Biochemical and Biophysical Research Communications* **148**, 817–826.

KELLER, B. U., HARTSHORNE, R. P., TALVENHEIMO, J. A., CATTERALL, W. A. & MONTAL, M. (1986). Sodium channels in planar lipid bilayers: channel gating kinetics of purified sodium channels modified by Batrachotoxin. *Journal of General Physiology* **88**, 1–23.

LACERDA, A. E. & BROWN, A. M. (1989). Nonmodal gating of cardiac calcium channels as revealed by dihydropyridines. *Journal of General Physiology* **93**, 1243–1273.

MCMANUS, O. B., BLATZ, A. L. & MAGLEBY, K. L. (1987). Sampling, log binning, fitting, and plotting durations of open and shut intervals from single channels and the effects of noise. *Pflügers Archiv* **410**, 520–553.

MCMANUS, O. B. & MAGLEBY, K. L. (1988). Kinetic states and modes of single large-conductance calcium-activated potassium channels. *Journal of Physiology* **402**, 79–120.

MCMANUS, O. B. & MAGLEBY, K. L. (1989). Kinetic time constants independent of previous single channel activity suggest Markov gating for a large conductance Ca-activated K channel. *Journal of General Physiology* **94**, 1037–1070.

MAGLEBY, K. L. & STEVENS, C. F. (1972). The effect of voltage on the time course of end-plate currents. *Journal of Physiology* **223**, 151–172.

MILLHAUSER, G. L., SALPETER, E. E. & OSWALD, R. E. (1988). Rate–amplitude correlation from single-channel records. A hidden structure in ion channel gating kinetics? *Biophysical Journal* **54**, 1165–1168.

MOCZYDLOWSKI, E. & LATORRE, R. (1983). Gating kinetics of Ca^{2+}-activated K^+ channels from rat muscle incorporated into planar lipid bilayers. Evidence for two voltage-dependent Ca^{2+} binding reactions. *Journal of General Physiology* **82**, 511–542.

NEHER, E. & SAKMANN, B. (1975). Voltage-dependence of drug-induced conductance in frog neuromuscular junction. *Proceedings of the National Academy of Sciences of the USA* **72**, 2140–2144.

NILIUS, B. (1988). Modal gating behaviour of cardiac sodium channels in cell-free membrane patches. *Biophysical Journal* **53**, 857–862.

NOVAK-HOFER, I. & LEVITAN, I. B. (1986). Regulation of ion channel activity by protein phosphorylation. *Progress in Brain Research* **69**, 107–118.

PATLAK, J. B., GRATION, K. A. & USHERWOOD, P. N. R. (1979). Single glutamate-activated channels in locust muscle. *Nature* **478**, 643–645.

PATLAK, J. B. & ORTIZ, M. (1986). Two modes of gating during the late Na^+ channel currents in frog sartorius muscle. *Journal of General Physiology* **87**, 305–326.

PATLAK, J. B., ORTIZ, M. & HORN, R. (1986). Open time heterogeneity during bursting of sodium channels in frog skeletal muscle. *Biophysical Journal* **49**, 773–777.

RAO, C. R. (1973). *Linear Statistical Inference and its Applications*. John Wiley, New York.

ROUX, B. & SAUVE, R. (1985). A general solution to the time interval omission problem applied to single channel analysis. *Biophysical Journal* **48**, 149–158.

SCHWARZ, T. L., TEMPEL, B. L., PAPAZIAN, D. M., JAN, Y. N. & JAN, L. Y. (1988). Multiple potassium-channel components are produced by alternate splicing at *Shaker* locus in *Drosophila*. *Nature* **331**, 137–142.

WEISS, D. S. (1988). Membrane potential modulates the activation of GABA-gated channels. *Journal of Neurophysiology* **59**, 514–527.

WEISS, D. S. & MAGLEBY, K. L. (1988). Investigating the steady-state voltage dependent kinetics of single ion channels: a case study for the fast chloride channel. *Biophysical Journal* **53**, 154a.

WHITE, M. M. & BEZANILLA, F. (1985). Activation of squid axon K^+ channels. Ionic and gating current studies. *Journal of General Physiology* **85**, 539–554.